Amyloid of Rnq1p, the basis of the [*PIN*$^+$] prion, has a parallel in-register β-sheet structure

Reed B. Wickner*†, Fred Dyda‡, and Robert Tycko†§

*Laboratory of Biochemistry and Genetics, National Institute of Diabetes Digestive and Kidney Diseases, National Institutes of Health, Building 8, Room 225, 8 Center Drive, MSC 0830, Bethesda, MD 20892-0830; ‡Laboratory of Molecular Biology, National Institute of Diabetes Digestive and Kidney Diseases, National Institutes of Health, Building 5, Room 303, 5 Memorial Drive, MSC 0560, Bethesda, MD 20892-0560; and §Laboratory of Chemical Physics, National Institute of Diabetes Digestive and Kidney Diseases, National Institutes of Health, Building 5, Room 112, 5 Memorial Drive, MSC 0520, Bethesda, MD 20892-0520

Contributed by Reed B. Wickner, December 20, 2007 (sent for review December 11, 2007)

The [PIN$^+$] prion, a self-propagating amyloid form of Rnq1p, increases the frequency with which the [*PSI*$^+$] or [URE3] prions arise *de novo*. Like the prion domains of Sup35p and Ure2p, Rnq1p is rich in N and Q residues, but *rnq1*Δ strains have no known phenotype except for inability to propagate the [PIN$^+$] prion. We used solid-state NMR methods to examine amyloid formed *in vitro* from recombinant Rnq1 prion domain (residues 153–405) labeled with Tyr-1–^{13}C (14 residues), Leu-1–^{13}C (7 residues), or Ala-3–^{13}C (13 residues). The carbonyl chemical shifts indicate that most Tyr and Leu residues are in β-sheet conformation. Experiments designed to measure the distance from each labeled residue to the next nearest labeled carbonyl showed that almost all Tyr and Leu carbonyl carbon atoms were ≈0.5 nm from the next nearest Tyr and Leu residues, respectively. This result indicates that the Rnq1 prion domain forms amyloid consisting of parallel β-strands that are either in register or are at most one amino acid out of register. Similar experiments with Ala-3–^{13}C indicate that the β-strands are indeed in-register. The parallel in-register structure, now demonstrated for each of the yeast prions, explains the faithful templating of prion strains, and suggests as well a mechanism for the rare hetero-priming that is [*PIN*$^+$]'s defining characteristic.

Three genetic criteria designed to identify infectious proteins (prions), resulted in the finding that two yeast nonchromosomal genes, [URE3] and [*PSI*$^+$], are prions of Ure2p and Sup35p, respectively (1). One of these *outre* genetic properties was that overproduction of the prion-forming protein should increase the frequency of the prion arising *de novo* (1). In fact, both [URE3] (1) and [*PSI*$^+$] (2) show this property. However, Derkatch *et al.* observed that, although overproduction of Sup35p induced the appearance of [*PSI*$^+$] in some strains, it was ineffective in doing so in others (3). This factor needed for [*PSI*$^+$]-inducibility behaved as a nonchromosomal gene, and so was dubbed [*PIN*$^+$] (3).

[*PIN*$^+$] has all of the genetic properties of a prion (4, 5), and was shown to be a self-propagating amyloid form of Rnq1p (4, 6), a protein rich in asparagine (N) and glutamine (Q), which had been shown to form self-propagating aggregates *in vivo* (7). Deletion of the *RNQ1* gene produces no evident phenotype (7), and the only known consequence of [*PIN*$^+$] is its priming effect on the other prions. Like its prion seeding effect, [*PIN*$^+$] seeds aggregate formation by polyQ (Huntingtin) (8, 9) and is thus required for Huntingtin-induced toxicity in yeast (9). Although Rnq1p and Sup35p form largely separate amyloid aggregates *in vivo* (10), it is likely that the mechanism of priming of [*PSI*$^+$] generation by [*PIN*$^+$] is a direct, but rare, addition of Sup35p to the fibrils of Rnq1p (11). Several variants of [*PIN*$^+$] are recognized (12, 13), distinguished by the efficiency with which they induce the appearance of [*PSI*$^+$] and [URE3]. As has been shown for [*PSI*$^+$] (14), it is likely that variants of [*PIN*$^+$] are different amyloid structures, although the precise nature of such differences remains unknown for any system at present.

Aggregates formed *in vitro* from Rnq1p are filamentous and stain with thioflavin T (7). Circular dichroism indicates that these aggregates are high in β-sheet content and, on exposure to proteinase K, show partial resistance (6). These studies indicate that the Rnq1p aggregates are amyloid fibers. Moreover, these fibers formed *in vitro* from recombinant Rnq1p are infectious for yeast spheroplasts, efficiently transmitting the [*PIN*$^+$] gene (6).

Because amyloid is neither soluble nor crystalline, neither solution NMR nor x-ray crystallography is suitable for elucidating its detailed structure, although the study of amyloid-like microcrystals of short oligopeptides has revealed details of packing and sidechain interactions that are relevant to amyloid structures (15, 16). Electron spin resonance studies have been used to study amylin (IAPP) and α-synuclein (17, 18) as well as amyloid of PrP (19). Solid-state NMR has been particularly useful for the elucidation of the structure of amyloids (reviewed in ref. 20). Selective labeling of particular amino acid residues with magnetic nuclear isotopes ^{13}C and ^{15}N, combined with pulse sequences designed to determine distances between labeled nuclei have provided structural information which has allowed construction of detailed evidence-based models of several amyloids. Various fragments of the Alzheimer's disease-linked Aβ have shown parallel and antiparallel structures (21–24). The full-length Aβ^{1-40} has a parallel in-register structure (25–27), as does amylin (17, 28), α-synuclein (18), and an amyloid of PrP (19). Solid-state NMR has also been used to obtain detailed information on the HETs protein prion domain (residues 218–289) (29, 30), and residues 105–115 of transthyretin (31).

The Ure2 and Sup35 prion proteins of yeast each consist of an N-terminal Q/N-rich amyloid-forming prion domain, a functional C-terminal domain and a connecting domain (refs. 32 and 33, reviewed in ref. 34). Solid-state NMR studies of amyloids of the prion domains of Sup35 (35) and Ure2p (36) as well as Ure2p$^{10-39}$ (37) have shown that each is a parallel, in-register β-sheet structure, meaning that, for example, residue 35 of one molecule is aligned opposite residue 35 of the preceding molecule and the subsequent molecule in the fibril.

Residues 153–405 of Rnq1p are quite Q/N rich (7) and are sufficient to serve as a prion domain (38), although some shorter segments contained in this region are also able to propagate the [*PIN*$^+$] prion (38). We report here that Rnq1$^{153-405}$ has a parallel in-register β-sheet structure, suggesting a mechanism for the cross-seeding of one prion by another.

Results

Fibril Formation by Rnq1$^{153-405}$. Fibers are reported to comprise only a small fraction of structures observed among aggregates of

Author contributions: R.B.W., F.D., and R.T. designed research; R.B.W., F.D., and R.T. performed research; R.B.W., F.D., and R.T. analyzed data; and R.B.W., F.D., and R.T. wrote the paper.

The authors declare no conflict of interest.

†To whom correspondence may be addressed. E-mail: wickner@helix.nih.gov or robertty@mail.nih.gov.

This article contains supporting information online at www.pnas.org/cgi/content/full/0712032105/DC1.

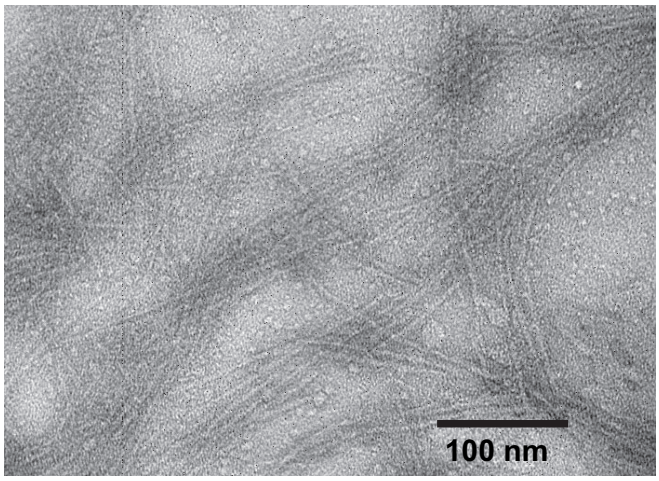

Fig. 1. Transmission electron micrographs of Rnq1$^{153–405}$ fibrils negatively stained with uranyl acetate.

Rnq1$^{132–405}$ formed in the absence of urea (11). Our fibril preparations, prepared in 4M urea, essentially as described by Sondheimer and Lindquist (7) and by Patel and Liebman (6) to make infectious aggregates, produced mostly fibrils (Fig. 1). Fibrils were regular, nonbranching with a diameter of 6–8 nm.

X-Ray Fiber Diffraction Shows β-Sheet Structure. Amyloid fibers of Rnq1$^{153–405}$ in water were exposed to x-rays and the diffraction pattern was observed (Fig. 2). A sharp line at $2\theta = 19°$ (19.038) indicates a primary spacing of 0.47 nm, the spacing between strands of a β-sheet. A broader peak at 10° (10.023) reflects a spacing of 0.87 nm, usually interpreted as reflecting the distance between layered β-sheets. The filamentous structure and the presence of the characteristic 0.47 nm reflection by x-ray fiber diffraction confirm that Rnq1$^{153–405}$ forms an amyloid structure.

Solid-State NMR Chemical Shifts Indicate β-Sheet Conformation. One-dimensional solid-state NMR spectra of wet fibrils of Rnq1$^{153–405}$ labeled with Tyr-1–^{13}C, Leu-1–^{13}C or Ala-3–^{13}C are shown in Fig. 3. Tyr-1–^{13}C labeled wet amyloid showed a single carbonyl peak at 172.2 ppm, whereas the shift expected for random coil structure is 174.2 ppm (39), suggesting that the Tyr residues detected are in β-sheet structure. The same fibrils, when dry, showed a second minor peak at 175.5 ppm whose intensity

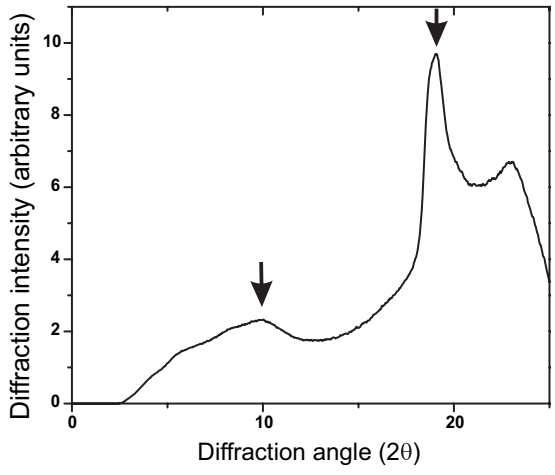

Fig. 2. x-ray fiber diffraction of fibrils of Rnq1$^{153–405}$. The major sharp peak at $2\theta = 19°$ indicates a distance of 4.7 Å, the distance between β strands.

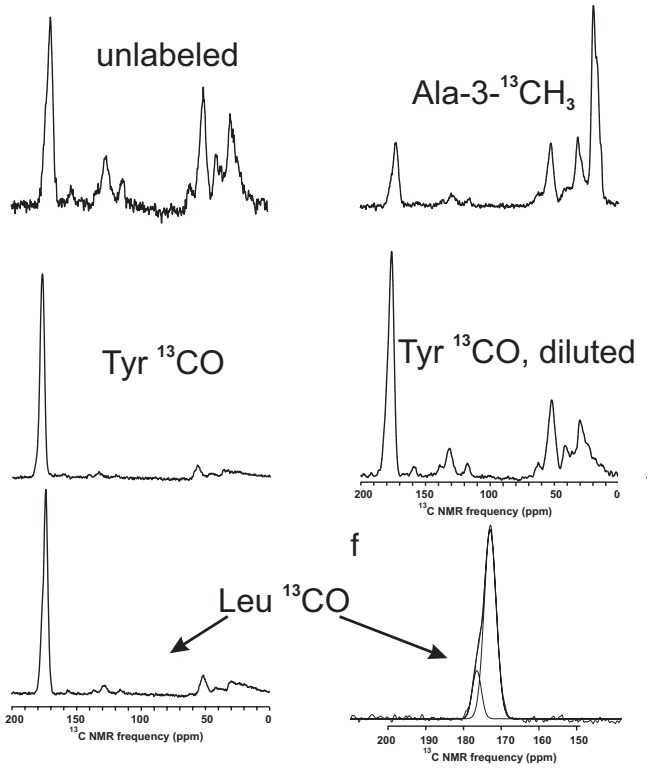

Fig. 3. Solid-state NMR spectra of samples used in this work. Spectra of Rnq1$^{153–405}$ labeled with Tyr-1–^{13}C, Leu-1–^{13}C, or Ala-3–^{13}C were recorded at 9.39 T at 20 kHz MAS. The carbonyl peak of the Leu-1–^{13}C-labeled sample was asymmetric, and could be deconvoluted into two Gaussian peaks.

suggests that 2.9 (of 15) residues are not in β-sheet structure, but are mobile when the sample is wet. Wet or dry amyloid formed of Rnq1$^{153–405}$ labeled with Leu-1–^{13}C gave two carbonyl peaks, a minor peak centered at 176.7 ppm, which is possibly due to a sum of the average of four natural abundance carbonyl carbons per molecule, and a major peak at 173.3 ppm (Fig. 3). The expected random coil chemical shift for Leu-1–^{13}C is 175.9 ppm, indicating that most Leu residues are in β-sheet structure.

As expected, only 67% labeling Rnq1$^{153–405}$ with Ala-3–^{13}C was achieved (see *Methods*), but it was critical for our purpose that substantial labeling of other residues be avoided. Indeed, in the 1D spectrum (Fig. 3) the methyl region (13 alanine atoms labeled 67% + 22 methyls in MIVLT residues with 1.1% natural abundance) gave an intensity of 100 (arbitrary units), from which the intensity per fully labeled residue is calculated to be 11.2 units. Based only on natural abundance, we expect the 365 carbonyl carbons to have a total intensity of 50 units and observed 27 units. The alpha carbon region (253 atoms $\times$ 0.011 $\times$ 11.2) should produce 31 units and we observed 31 units. These results suggest that there was little leakage of label into residues other than alanine.

PITHIRDS-CT Data Indicate 0.5-nm Nearest Neighbor ^{13}C–^{13}C Distances for Most Labeled Sites. In solution NMR, differences in local magnetic fields due to chemical shift anisotropies and dipole–dipole couplings are averaged out by rapid molecular tumbling and very sharp lines result. In solid-state NMR, there is little molecular motion and so magic-angle spinning (MAS) of the sample as a whole is necessary to prevent these effects from producing excessive line broadening and dephasing of spins. However, because of their sharp distance dependence (as $1/r^3$), these same dipole–dipole couplings are useful for measuring distances and bond angles. Thus, ''dipolar recoupling'' methods

have been developed to restore some of the dipole–dipole couplings that would otherwise be averaged out by MAS. The dipolar recoupling method used here is called PITHIRDS-CT and has the virtue of being relatively insensitive to errors in pulse calibration (40). A π pulse each rotation lasting 1/3 of the rotation period (hence PITHIRDS) recouples the ^{13}C–^{13}C interactions that would otherwise have been averaged out by MAS.

The prion domain of Rnq1 (residues 153–405) has 15 tyrosine and 7 leucine residues, each evenly distributed so that no two tyrosines or two leucines have fewer than two intervening residues (>0.9 nm). The rate of decay of the ^{13}C NMR signal is proportional to $1/r^3$ where r is the distance to the next nearest ^{13}C atom. In fibers made from molecules labeled with Leu-1-^{13}C or with Tyr-1–^{13}C, the signal decay is rapid indicating, based on the standard curves, a distance of ≈0.5 nm from the next nearest labeled carbonyl carbon (Fig. 4*A*). Rnq1$^{153–405}$ fibrils labeled with Leu-1–^{13}C were dissolved in 8 M guanidine HCl and then precipitated with methanol. The resulting nonspecific aggregate showed a substantially decreased rate of signal decay, indicating that the specific structure of the fibers is responsible for the rapid decay of signal, not simple aggregation (Fig. 4*A*).

The natural abundance (1.1%) ^{13}C in an unlabeled sample shows the expected slow signal decay because the rare ^{13}C atoms are far from each other (Fig. 4*B*). Forming amyloid from fully Tyr-1–^{13}C-labeled Rnq1$^{153–405}$ diluted with four parts of unlabeled Rnq1$^{153–405}$ decreased the rate of decay dramatically, indicating that the decay is due to intermolecular interactions and not intramolecular interactions (Fig. 4*B*). Assuming that the amyloid structure is a parallel in-register β-sheet, each labeled molecule is adjacent to two others. The "diluted, calc." curve was calculated assuming that only if both adjacent molecules are unlabeled will the labeled molecule show the decay rate of the natural abundance (unlabeled) molecule. The decay rate of the Tyr-1–^{13}C diluted sample showed a rate of signal decay essentially the same as this expected rate (Fig. 4*B*).

The data shown in Fig. 4 were collected with hydrated samples. Similar data with dried samples show slightly less rapid decay [supporting information (SI) Fig. 7], suggesting that a fraction of labeled residues are not in parallel in-register β-sheet structure and become mobile, and thus invisible, on hydration. To estimate this fraction, we assume the non-β-sheet residues decay at the rate of natural abundance ^{13}C (Fig. 4*B*). With this assumption, the data indicate that 3.7 of 15 tyrosine and one of seven leucine residues are not in β-sheet, consistent with the results of 1D spectra described above.

Ala-3–^{13}C-Labeled Rnq1$^{153–405}$ Rapid Signal Decay Shows Parallel In-Register Structure. Although the results with Tyr-1–^{13}C and Leu-1–^{13}C molecules strongly suggest an in-register parallel β-sheet structure, the results are actually compatible with a structure out of register by a single amino acid residue. However, successive "R" groups of amino acids in a β-strand point approximately in opposite directions, so that Rnq1$^{153–405}$ labeled in the methyl group of the 13 Ala residues would show rapid decay indicative of a 0.5-nm nearest neighbor distance for the in-register case, but a much slower decay indicating a >0.8 nm distance if the structure is out of register by a single residue. In fact, the rapid decay indicating in-register structure was observed (Fig. 4*C*).

Two-Dimensional ^{13}C–^{13}C, ^{1}H–^{13}C, and ^{15}N–^{13}C Solid-State NMR Spectra of Rnq1$^{153–405}$. Two dimensional NMR data can indicate the degree of sample heterogeneity, which residues are structured, and, potentially, detailed atomic level structure. Fig. 5 shows the aliphatic part of a ^{13}C–^{13}C 2D experiment (see *Methods*) using uniformly ^{13}C,^{15}N-labeled Rnq1p$^{153–405}$. The complete 2D ^{13}C–^{13}C, ^{15}N–^{13}C and ^{1}H-^{13}C NMR spectra are shown in SI Figs. 8–10. Because Rnq1p$^{153–405}$ has 67 Q, 42 G, 41 N, and 39 S residues, the spectrum is dominated by several areas of overlapping signals (Fig. 5*A*). However, two alanine $\alpha\beta$ resonances and the two threonine $\alpha\beta$ peaks are detected with peak widths

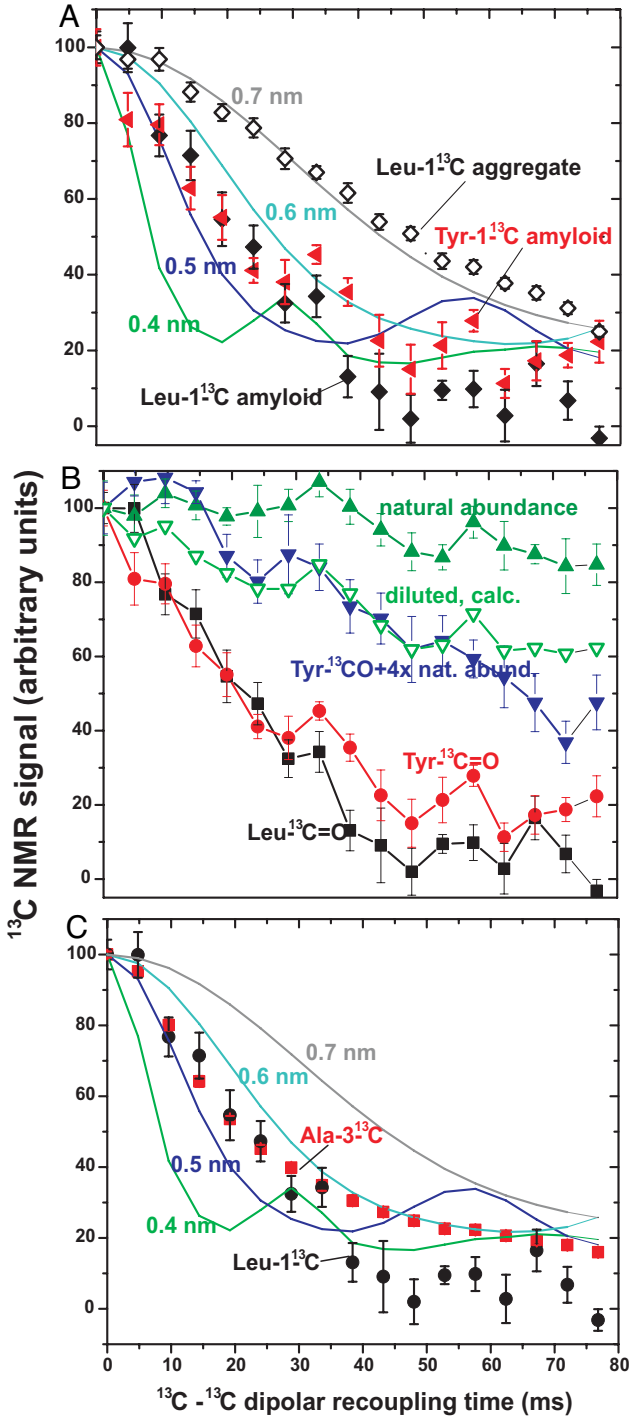

Fig. 4. Dipolar recoupling experiments indicate parallel structure of Rnq1p$^{153–405}$. (*A*) Dipolar recoupling experiments with Rnq1$^{153–405}$ labeled with Leu-1–^{13}C or Tyr-1–^{13}C. Rate of signal decay is inversely proportional to the cube of the distance to the next nearest ^{13}C. Standard curves for 0.4, 0.5, 0.6, and 0.7 nm are simulations carried out as described (28). (*B*) Dilution of Tyr-1–^{13}C-labeled Rnq1$^{153–405}$ with unlabeled Rnq1$^{153–405}$ reduces the signal decay indicating that the next nearest Tyr-1–^{13}C is on another Rnq1$^{153–405}$ molecule. Natural abundance shows the decay from an unlabeled sample with the natural 1.1% ^{13}C signal. (*C*) The rate of signal decay of Ala-3–^{13}C indicates an in-register β-sheet structure (see text).

BIOPHYSICS

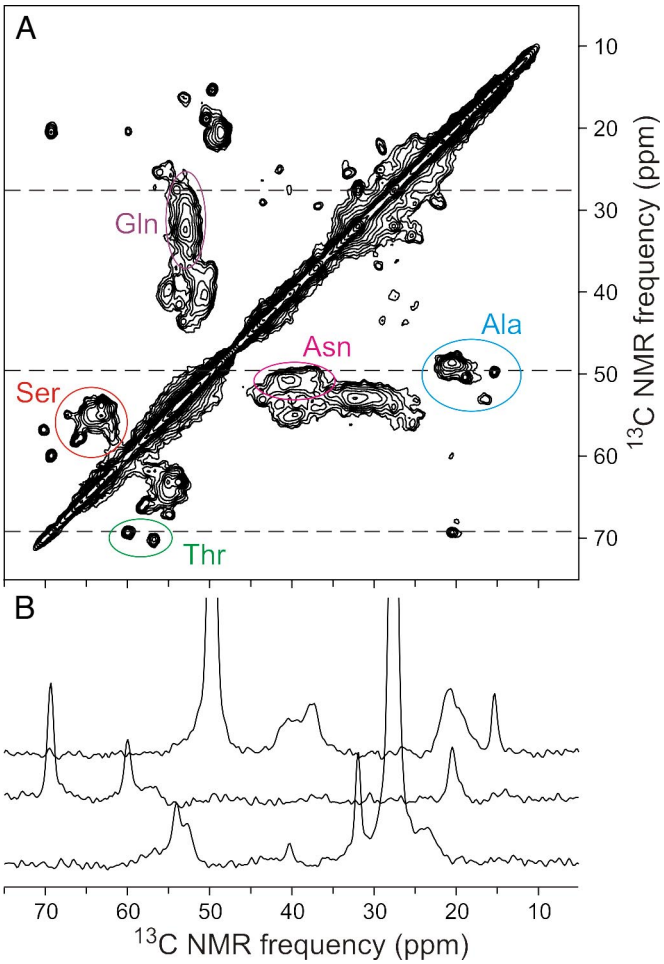

Fig. 5. Two-dimensional NMR of Rnq1$^{153–405}$. (*A*) Aliphatic region of 2D ^{13}C–^{13}C spectrum of U–^{15}N,^{13}C–Rnq1$^{153–405}$ fibrils, with partial residue-type assignments of C_α/C_β crosspeaks, obtained at a 17.00-kHz MAS frequency with a total of 55,296 scans and a maximum *t*1 value of 4.896 ms. Contour levels increase by successive factors of 1.5. (*B*) One-dimensional slices from the 2D spectrum, at positions indicated by dashed lines.

≈0.7 ppm, indicating a relatively homogeneous structure at those sites, compared with many amyloids that show peak widths of 1.5–2.5 ppm. Although there are two proline residues, no peaks attributable to proline were identified, suggesting that these residues were mobile or unstructured.

Most Ala $\alpha\beta$ cross-peaks (Fig. 5*A*) have α resonances below and β resonances above the random coil values of 50.8 and 17.4 (relative to TMS), respectively, indicating β-sheet structure. The two isolated peaks are apparently not in β-sheets. For Thr (random coil values $\alpha = 60.1$, $\beta = 68.1$), one residue has shifts suggesting β-sheet and the other does not (Fig. 5*A*). Likewise for Ser (random coil $\alpha = 56.6$, $\beta = 62.1$), most intensity appears to be in β-sheet, but a few residues are not. Most Asn (random coil $\alpha = 51.4$, $\beta = 37.2$) and Gln (random coil $\alpha = 54.0$, $\beta = 27.7$) intensity is consistent with β-sheet, but the many residues and broad distribution make it impossible to rule out some non-β-sheet structure (Fig. 5*A*).

Discussion

A self-propagating amyloid of Rnq1p is the basis of the [*PIN*$^+$] prion of *Saccharomyces cerevisiae*. These asparagine/glutamine-rich fibers apparently prime the polymerization of the similarly N/Q-rich prion domains of the Sup35 and Ure2 proteins, initiating formation of the [*PSI*$^+$] and [URE3] prions, respectively.

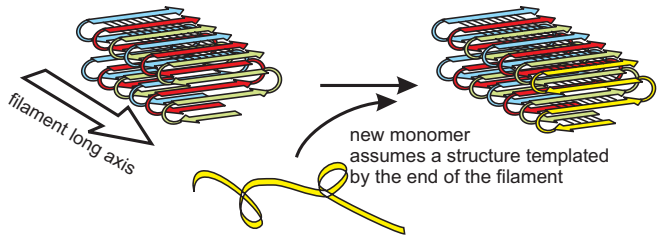

Fig. 6. Schematic model of fibrils of Rnq1p$^{153–405}$. There is no information on the lengths or locations of loop regions or on the nature of the contacts between sheets.

Here we examine the structure of amyloid of Rnq1p, formed under conditions (6) that produce infectious material. Solid-state NMR measurements of nearest-neighbor distances between tyrosine or leucine residues show distances of ≈0.5 nm, indicative of a parallel in-register β-sheet structure, but consistent with a structure out of register by a single amino acid. Similar experiments with Rnq1$^{153–405}$ labeled with Ala-3–^{13}C show that the structure is, in fact, in-register. Infectious amyloid of Sup35NM (35) and the prion domain of Ure2p (36) likewise have a parallel in-register β-sheet structure, suggesting that [*PIN*$^+$] priming of [*PSI*$^+$] or [URE3] is a simple direct (rare) substitution of a Sup35 or Ure2 molecule for a Rnq1 molecule at a growing end of a fibril.

In the parallel in-register β-sheet structure, each residue of the prion domain contacts the same residue in the molecule that was laid down before it and the same residue in the next molecule to join the fibril (Fig. 6). This provides the possibility of passing on structural variations, such as locations of turns of the sheet, lengths of loops, or irregularities in the structure, from parent molecules (already in the fiber) to daughter molecules newly being laid down. This is the essential "templating" mechanism that must be present for these proteins to act as genes. This can explain the prion "variants," cases where the identical amino acid sequence produces different phenotypes or prion stabilities, doubtless due to differing details of the amyloid structure.

This structure also indicates that the sequence of events is not, as often suggested, a primary conformational change of the prion protein followed by aggregation. For example, the monomeric protein could not adopt the structure it has in the fibril because the backbone bonds that drive the structure in the fibril are all intermolecular. It seems evident that the conformational change is coincident with and a consequence of the new molecule joining the fibril, and the details of the conformational change are directed by the structure of the end of the fibril (Fig. 6).

Although amyloid of Rnq1$^{153–405}$ clearly has a parallel in-register β-sheet structure, two-dimensional ^{13}C–^{13}C NMR experiments show line widths suggestive of significant structural heterogeneity among fibrils, consistent with the known existence of multiple [*PIN*$^+$] prion variants (12). Most or all of the variants must share the parallel in-register β-sheet structure as a common feature, but the locations of turns or other details may differ among fibrils.

Although amyloids of a number of peptide fragments have been shown to be antiparallel structures, most natural amyloids and amyloids of the prion domains of each of the yeast prions has a parallel in-register structure. The (so far exceptional) HETs prion domain amyloid is proposed to be an intramolecular "pseudo" parallel in-register β-sheet, but in some ways also resembles a β-helix (29, 30).

Further work will be required to more completely define the Rnq1p amyloid structure, the structural differences among prion strains, the structural determinants of interactions with chaperones, and other cellular components.

Methods

Protein Preparation. Rnq1p$^{153–405}$ with C-terminal His_6 tag was labeled and expressed in *E. coli* and purified as described in *SI Text*.

Electron Microscopy. The formation of fibrils by Rnq1p was confirmed by electron microscopy of negatively stained samples. A fibril suspension was applied to a carbon-coated copper grid for ≈2 min, washed briefly with H_2O, stained for ≈2 min with 2% uranyl acetate, blotted, and air dried. The stained samples were examined with an FEI Morgagni transmission electron microscope operating at 80 kV.

Mass Spectrometry. Incorporation of alanine-3–^{13}C was estimated by mass spectrometric measurements of the chymotryptic peptide SSLASMAQSY, which was ≈67% labeled. There was no evidence for incorporation of ^{13}C into other residues, a conclusion supported by NMR data (see *Results*).

X-Ray Fiber Diffraction. Amyloid fibers of Rnq1$^{153–405}$ were washed extensively with water and packed wet into a 0.7-mm-diameter, thin walled boron-rich glass capillary by centrifugation. The packed fibers were placed in a 0.15418 nm wavelength x-ray beam generated by a rotating anode source operated at 50 kV and 100 mA, coupled with a multilayer focusing optics. Diffraction data were collected in 120-min exposures, during which the sample was continuously rotated around an axis perpendicular to the beam. Diffraction data were recorded on an RaxisIV 2-dimensional imaging plate detector placed 15 cm from the capillary. Background data were collected similarly, but exposing a part of the same capillary that was free of fiber but was filled with water. The data were converted to intensity vs. 2θ plots by circular summation around the center of the two-dimensional images using the R-axis Display Program (Rigaku Americas). Background was subtracted and the resulting plots were displayed by Origin 7 (OriginLab)

Solid-State NMR Methods. Solid-state NMR experiments on selectively labeled Rnq1p$^{153–405}$ were carried out at 9.39 T (100.4 MHz ^{13}C NMR frequency) using an InfinityPlus spectrometer (Varian) and magic angle spinning (MAS) NMR probes (Varian) with 3.2 mm diameter rotors. All measurements were at room temperature. ^{13}C NMR spectra were recorded at an MAS frequency of 20.00 kHz with ^{1}H–^{13}C cross-polarization (41) and two-pulse phase-modulated ^{1}H decoupling (42). The dipolar recoupling measurements were carried out at an MAS frequency of 20.00 kHz using the PITHIRDS-CT method (40). Pulsed spin-lock detection was used for improved signal-to-noise ratio (43). Rnq1$^{153–405}$ fibrils were washed extensively with H_2O, lyophilized, packed into rotors (4- to 6-mg sample masses) and rehydrated by addition of ≈5 μl of H_2O. Each PITHIRDS-CT data point is the result of 512–576 scans with a 4-s recycle delay.

The original PITHIRDS-CT data, $S_{raw}(t)$ were corrected for the 1.1% natural abundance of ^{13}C as follows: (*i*) PITHIRDS-CT data were recorded for an unlabeled sample of Rnq1$^{153–405}$ (Fig. 4*B*) and, assuming linear decay, the natural abundance signal is $S_{na} = 100 - 0.208\,t$, where t is the effective dipolar dephasing time in milliseconds; (*ii*) the number of natural abundance ^{13}C nuclei per Rnq1$^{153–405}$ molecule, N_{na}, is 0.011 × (total sites − labeled nuclei), where total sites is 372 carbonyls or 35 methyls. Labeled nuclei, N_{label}, was 7, 15 and 8.7 for Leu, Tyr, and Ala, respectively, taking account of the 67% labeling of alanines. The corrected PITHIRDS-CT data were $S(t) = [S_{raw}(t) - f_{na}\,S_{na}(t)]/(1 - f_{na})$, where $f_{na} = N_{na}/(N_{na} + N_{label})$ and $S_{raw}(0) = 100$. Standard errors are shown.

Measurements on uniformly ^{15}N,^{13}C-labeled Rnq1 (U-^{15}N,^{13}C-Rnq1) fibrils were performed in a 17.6 T field (747.9 MHz ^{1}H NMR frequency, 188.1 MHz ^{13}C NMR frequency, 75.8 MHz ^{15}N NMR frequency), using a Varian Infinity spectrometer console and a three-channel MAS probe with 1.8 mm rotor diameters (produced by the research group of Ago Samoson, National Institute of Chemical Physics and Biophysics, Tallinn, Estonia). Lyophilized U–^{15}N,^{13}C–Rnq1 fibrils were packed into the MAS rotor and then rehydrated by addition of deionized water until the sample appeared translucent when viewed in the rotor with strong illumination. 2D ^{13}C–^{13}C and ^{15}N–^{13}C NMR spectra were recorded at a 17.00 kHz MAS frequency. Two-dimensional ^{1}H-^{13}C spectra were recorded at a 40.00 kHz MAS frequency. A 2.824-ms (48 rotor periods) finite-pulse RFDR sequence was applied in the mixing period of 2D ^{13}C-^{13}C measurements, with 18.0-μs ^{13}C π pulses. The mixing period in 2D ^{15}N–^{13}C measurements consisted of a 6.00-ms ^{15}N–^{13}C cross-polarization period, optimized for polarization transfer to α-carbons, followed by a 20-ms ^{13}C–^{13}C spin diffusion period. A 200-μs ^{1}H–^{13}C cross-polarization period was used for mixing in 2D ^{1}H–^{13}C measurements. Proton decoupling fields in all measurements were 110 kHz.

ACKNOWLEDGMENTS. R.B.W. thanks Kent Thurber, Anant Paravastu, Sorin Luca, and Kan Hu for frequent advice, encouragement, and rescue; Frank Shewmaker for advice on protein purification; and Eric Anderson for mass spectrometry. This work was supported by the Intramural Program of the National Institute of Diabetes Digestive and Kidney Diseases of the National Institutes of Health.

1. Wickner RB (1994) [URE3] as an altered *URE2* protein: Evidence for a prion analog in *S. cerevisiae*. *Science* 264:566–569.
2. Chernoff YO, Derkach IL, Inge-Vechtomov SG (1993) Multicopy SUP35 gene induces de-novo appearance of psi-like factors in the yeast *Saccharomyces cerevisiae*. *Curr Genet* 24:268–270.
3. Derkatch IL, Bradley ME, Zhou P, Chernoff YO, Liebman SW (1997) Genetic and environmental factors affecting the *de novo* appearance of the [*PSI*+] prion in *Saccharomyces cerevisiae*. *Genetics* 147:507–519.
4. Derkatch IL, *et al.* (2000) Dependence and independence of [*PSI*$^{+}$] and [*PIN*$^{+}$]: A two-prion system in yeast? *EMBO J* 19:1942–1952.
5. Derkatch IL, Bradley ME, Hong JY, Liebman SW (2001) Prions affect the appearance of other prions: The story of [PIN]. *Cell* 106:171–182.
6. Patel BK, Liebman SW (2007) ''Prion proof'' for [PIN+]: Infection with in vitro-made amyloid aggregates of Rnq1p-(132–405) induces [PIN+]. *J Mol Biol* 365:773–782.
7. Sondheimer N, Lindquist S (2000) Rnq1: an epigenetic modifier of protein function in yeast. *Mol Cell* 5:163–172.
8. Osherovich LZ, Weissman JS (2001) Multiple Gln/Asn-rich prion domains confer susceptibility to induction of the yeast *[PSI+]* prion. *Cell* 106:183–194.
9. Merrin AB, *et al.* (2002) Huntingtin toxicity in yeast model depends on polyglutamine aggregation mediated by a prion-like protein Rnq1. *J Cell Biol* 157:997–1004.
10. Bagriantsev S, Liebman SW (2004) Specificity of prion assembly in vivo. [PSI+] and [PIN+] form separate structures in yeast. *J Biol Chem* 279:51042–51048.
11. Vitrenko YA, Gracheva EO, Richmond JE, Leibman SW (2007) Visualization of aggregation of the Rnq1 prion domain and cross-seeding interactions with Sup35NM. *J Biol Chem* 282:1779–1787.
12. Bradley ME, Edskes HK, Hong JY, Wickner RB, Liebman SW (2002) Interactions among prions and prion ''strains'' in yeast. *Proc Natl Acad Sci USA* 99(Suppl 4):16392–16399.
13. Bradley ME, Liebman SW (2003) Destabilizing interactions among [*PSI*+] and [*PIN*+] yeast prion variants. *Genetics* 165:1675–1685.
14. Tanaka M, Chien P, Naber N, Cooke R, Weissman JS (2004) Conformational variations in an infectious protein determine prion strain differences. *Nature* 428:323–328.
15. Nelson R, *et al.* (2005) Structure of the cross-β spine of amyloid-like fibrils. *Nature* 435:773–778.
16. Sawaya MR, *et al.* (2007) Atomic structures of amyloid cross-beta spines reveal varied steric zippers. *Nature* 447:453–457.
17. Jayasinghe SA, Langen R (2004) Identifying structural features of fibrillar islet amyloid polypeptide using site-directed spin labeling. *J Biol Chem* 279:48420–48425.
18. Der-Sarkissian A, Jao CC, Chen J, Langen R (2003) Structural organization of α-synuclein fibrils studied by site-directed spin labeling. *J Biol Chem* 278:37530–37535.
19. Cobb NJ, Sonnichsen FD, Mchaourab H, Surewicz WK (2007) Molecular architecture of human prion protein amyloid: a parallel, in-register β-structure. *Proc Natl Acad Sci USA* 104:18946–18951.
20. Tycko R (2006) Molecular structure of amyloid fibrils: Insights from solid-state NMR. *Q Rev Biophys* 1:1–55.
21. Lansbury PT, Jr, *et al.* (1995) Structural model for the beta-amyloid fibril based on interstrand alignment of an antiparallel-sheet comprising a C-terminal peptide. *Nat Struct Biol* 2:990–998.
22. Benzinger TL, *et al.* (1998) Propagating structure of Alzheimer's beta-amyloid(10–35) is parallel beta-sheet with residues in exact register. *Proc Natl Acad Sci USA* 95:13407–13412.
23. Gregory DM, *et al.* (1998) Dipolar recoupling NMR of biomolecular self-assemblies: Determining inter- and intrastrand distances in fibrilized Alzheimer's β-amyloid peptide. *Solid State Nucl Magn Reson* 13:149–166.
24. Burkoth TS, *et al.* (2000) Structure of the β-amyloid(10–35) fibril. *J Am Chem Soc* 122:7883–7889.
25. Antzutkin ON, *et al.* (2000) Multiple quantum solid-state NMR indicates a parallel, not antiparallel, organization of beta-sheets in Alzheimer's beta-amyloid fibrils. *Proc Natl Acad Sci USA* 97:13045–13050.
26. Petkova AT, *et al.* (2002) A structural model for Alzheimer's beta-amyloid fibrils based on experimental constraints from solid state NMR. *Proc Natl Acad Sci USA* 99:16742–16747.
27. Petkova AT, Yau WM, Tycko R (2006) Experimental constraints on quaternary structure in Alzheimer's beta-amyloid fibrils. *Biochemistry* 45:498–512.
28. Luca S, Yau W-M, Leapman R, Tycko R (2007) Peptide conformation and supramolecular organization in amylin fibrils: Constraints from solid-state NMR. *Biochemistry* PMID: 17979302.
29. Ritter C, *et al.* (2005) Correlation of structural elements and infectivity of the HET-s prion. *Nature* 435:844–848.
30. Siemer AB, *et al.* (2006) 13C, 15N resonance assignment of parts of the HET-s prion protein in its amyloid form. *J Biomol NMR* 34:75–87.

31. Jaroniec CP, *et al.* (2004) High-resolution molecular structure of a peptide in an amyloid fibril determined by magic angle spinning NMR spectroscopy. *Proc Natl Acad Sci USA* 101:711–716.
32. TerAvanesyan A, Dagkesamanskaya AR, Kushnirov VV, Smirnov VN (1994) The *SUP35* omnipotent suppressor gene is involved in the maintenance of the non-Mendelian determinant [psi+] in the yeast *Saccharomyces cerevisiae*. *Genetics* 137:671–676.
33. Masison DC, Wickner RB (1995) Prion-inducing domain of yeast Ure2p and protease resistance of Ure2p in prion-containing cells. *Science* 270:93–95.
34. Ross ED, Minton AP, Wickner RB (2005) Prion domains: Sequences, structures and interactions. *Nat Cell Biol* 7:1039–1044.
35. Shewmaker F, Wickner RB, Tycko R (2006) Amyloid of the prion domain of Sup35p has an in-register parallel β-sheet structure. *Proc Natl Acad Sci USA* 103:19754–19759.
36. Baxa U, *et al.* (2007) Characterization of β-sheet structure in Ure2p1–89 yeast prion fibrils by solid state nuclear magnetic resonance. *Biochemistry* 46:13149–13162.
37. Chan JCC, Oyler NA, Yau W-M, Tycko R (2005) Parallel β-sheets and polar zippers in amyloid fibrils formed by residues 10–39 of the yeast prion protein Ure2p. *Biochemistry* 44:10669–10680.
38. Vitrenko YA, Pavon ME, Stone SI, Liebman SW (2007) Propagation of the [*PIN*$^+$] prion by fragments of Rnq1 fused to GFP. *Curr Genet* 51:309–319.
39. Wishart DS, Bigam CG, Holm A, Hodges RS, Sykes BD (1995) H-1, C-13 and N-15 random coil NMR chemical-shifts of the common amino-acids. 1. Investigations of Nearest-Neighbor Effects. *J Biomol NMR* 5:67–81.
40. Tycko R (2007) Symmetry-based constant-time homonuclear dipolar recoupling in solid-state NMR. *J Chem Phys* 126:064506.
41. Pines A, Gibby MG, Waugh JS (1973) Proton-enhanced NMR of dilute spins in solids. *J Chem Phys* 59:569–590.
42. Bennett AE, Rienstra CM, Auger M, Lakshmi KV, Griffin RG (1995) Heteronuclear decoupling in rotating solids. *J Chem Phys* 103:6951–6958.
43. Petkova AT, Tycko R (2002) Sensitivity enhancement in structural measurements by solid state NMR through pulsed spin locking. *J Magn Reson* 155:293–299.